Recycling spent lead acid batteries into aqueous zinc-ion battery material with ultra-flat voltage platforms

Chun Lin,[1,2] Yue Chen,[1,4,5 *] Weijian Zhang ,[1,3] Jiaxin Li,[1,2*] Yingbin Lin,[1,2] Oleg V. Kolosov,[4,5] and Zhigao Huang[1,3 *]

[1]*College of Physics and Energy, Fujian Normal University, Fujian Provincial Key Laboratory of Quantum Manipulation and New Energy Materials, Fuzhou， 350117, China*

[2]*Fujian Provincial Engineering Technical Research Centre of Solar-Energy Conversion and Stored Energy, Fuzhou， 350117, China*

[3]*Fujian Provincial Collaborative Innovation Centre for Advanced High-Field Superconducting Materials and Engineering, Fuzhou, 350117, China*

[4]*Physics Department, Lancaster University, Lancaster, LA1 4YB, UK*

[5]*The Faraday Institution, Quad One, Harwell Science and Innovation Campus, Didcot, OX11 0RA, UK*

*Corresponding authors: y.chen102@lancaster.ac.uk, ljx0721@qq.com, zghuang@fjnu.edu.cn

Abstract:

The harmless disposal of lead paste in the spent lead-acid batteries (LABs) remains an enormous challenge in traditional pyrometallurgical recycling. Here, we introduced a hydrometallurgical method for the recycling of the spent LABs' waste to obtain the *β*-PbO as a novel zinc ion batteries (ZIBs) active material. The obtained *β*-PbO exhibits ultra-flat charge/discharge voltage platforms (0.21 mV/(mAh g^{-1})) and stable specific capacity. During the charge/discharge, the *β*-PbO spontaneously triggers the formation of $(ZnSO_4)[Zn(OH)_2]_3 \cdot 5H_2O$ (ZHS) micro-sheets as a surface passivation layer. Moreover, the *ex-situ* X-ray spectra reveal that the reversible phase transformation occurs between $PbSO_4$ and Pb with the assistance of ZHS by adjusting the PH value on the electrode-electrolyte interface. The synergistic two-phase-reaction mechanism generates ultra-flat voltage platforms upon the charge/discharge. This "energy-saving and environment-friendly" recycling route eliminates

the major source of emission of pollution particulates/gases compared to the traditional pyrometallurgical recycling, while at the same time replacing energy-consuming and environmentally detrimental processes of synthesis of current ZIBs cathodes.

Keywords: *Aqueous zinc ion battery, Hydrometallurgical battery recycling, Lead oxide, Ultra-flat voltage platform*

1. Introduction

In the past few decades, lithium-ion batteries (LIBs) have been widely explored and used because of their higher energy density compared to other secondary batteries [1-5]. However, the processing costs, safety issues, limited lithium resources, and environmental issues caused by spent LIBs have caused many concerns [6,7]. To alleviate the reliance on lithium-ion batteries, scientists have renewed interest in alternative energy storage devices [8-12], especially developing the aqueous rechargeable batteries (ARB) due to their low cost and high operational safety [13-15].

Among these aqueous rechargeable batteries, zinc ion batteries (ZIBs) which have good water compatibility, natural abundance and low redox potential (−0.76 V vs. SHE), are particularly attractive [16-18]. To date, the cathode materials for aqueous zinc-ion batteries mainly include manganese-based oxides (MnO_2 with different crystal structures [19-22], Mn_2O_3 [23], Mn_3O_4 [24,25], $ZnMn_2O_4$ [26]), vanadium-based oxides (VO_2 [27], V_2O_5 [28,29], $Na_{0.33}V_2O_5$[30], $Ca_{0.25}V_2O5{\cdot}nH_2O$ [31], LiV_3O_8 [32], $Zn_2V_2O_7$ [33]), Prussian blue analogs [34], and polyanionic compounds [35]. The capacity of manganese-based oxides is restricted by manganese dissolving [19], and Zn^{2+} diffusion inside vanadium-based oxides is affected by the strong electrostatic interaction between divalent Zn^{2+} ions and the host lattice [28,29,37,38]. Besides, the stable and flat charging and discharging platform, which is critical to the battery power output and energy density [39-41], has rarely been observed in these cathode materials. More significantly, the synthesis of these materials requires either energy-consuming calcination processes or wet-chemical synthesis methods with potential water pollution. Synthesizing the ZIB materials with a stable output voltage platform and performance by environment-friendly methods remains a substantial challenge.

The ideal candidate material for high performance aqueous ZIBs should be compatible with the aqueous electrolyte and have stable charge/discharge voltage platforms. According to the Gibbs phase law, a battery material that shows a direct two-phase reaction between the initial and final phases can deliver flat voltage platforms. We therefore focus on the electrode materials of lead acid batteries (LABs) which is one of the most successful aqueous energy storage systems based on the two-phase reaction mechanism ($PbO_2 \leftrightarrow PbSO_4$ for cathode and $Pb \leftrightarrow PbSO_4$ for the anode). Significantly, to reduce the energy consumption and pollution that may be caused by the material synthesis processes, we recovered the lead resource from lead paste inside the spent LABs and used it as an aqueous ZIBs material. This is also significant for LAB recycling since the lead paste is the least reusable part of spent LABs.

LABs have been widely used for backup power supplies in cell phone towers and powering vehicle starters. As a traditional secondary battery with about 60% market share, the projected LAB manufacturing market value was estimated to reach about 80 billion by 2026 [42,43]. However, nowadays, the increased consumption and production of LABs, together with various types of battery products, are generating more waste batteries. This sharply increases the demand for battery recycling and safe disposal. Especially, in LAB recycling, there is a growing need to develop new recycling methods for lead paste, because the traditional pyrometallurgical recycling route for lead paste causes serious environmental pollution as well as health impacts on the human body due to lead exposure [44]. Although the environment more friendly electrowinning method has been introduced as an alternative for the desulfuration of lead sulfide in lead paste, the high energy consumption during the electroextraction hinders its further promotion. By contrast, it is worth mentioning that the desulfuration of lead sulfide can be effectively achieved by using an alkaline/acid solution as the leaching agent in the hydrometallurgical process [43]. Introducing the hydrometallurgical LAB recycling process to produce new energy storage materials has been reported before. For example, the recovered and recycled lead compounds have been applied as active cathode/anode materials in various types of batteries, including lead-carbon batteries [45] and Li-S batteries [46]. But to the best

of our knowledge, no studies have attempted to apply the recycled byproduct of spent LABs as novel ZIBs materials.

In this work, we introduced a one-step hydrometallurgical conversion method to obtain the *β*-PbO from the lead paste in spent LABs. The obtained *β*-PbO/Zn cell using an aqueous $ZnSO_4$ electrolyte was first validated as an electrochemical active and reversible system. The *β*-PbO electrode exhibits a stable charge/discharge platform and the discharge specific capacity up to 80 mAh g^{-1} at 1A g^{-1} during the 200 cycles. In addition, the charge transfer mechanism was studied in detail by *ex-situ* X-rays Diffraction (XRD), X-ray photoelectron spectroscopy (XPS) and in situ pH meter. This work provides a new perspective for sustainable materials as new ZIBs active materials.

2. Experimental section

2.1 Material Preparation.

The lead acid battery (CAMEL GROUP CO, China) was charged and discharged at 1using the LANHE CT2001A battery test system within a voltage window of 3-5 V. We cycled the lead-acid battery until the battery is completely attenuated (Supplementary Information, SI, Figure S1). Subsequently, following the industrial recycling routine, the spent lead-acid battery was crushed into pieces and then inserted into a vat, in which the heavy materials and lead dropped to the bottom and plastic pieces floated. For the solid waste, the lead meshes/fragments and polypropylene plastic pieces are removed using a Gauze filter and then went through the different industrial recycling procedures, leaving the lead paste as the last waste to be further recycled (Desulfurization). The lead paste in the fully discharged battery mainly consisted of lead sulfide and lead oxide that was collected and dried in the oven for the subsequent hydrometallurgical desulfurization. The NaOH solution and lead paste were mixed for desulfurization treatment at 80℃ for 100 minutes, followed by solid-liquid separation and washing with deionized water. At the same time, the influence of NaOH concentration (0.5 mol/L, 1 mol/L, 2 mol/L) and temperature (30℃, 60℃, 80℃) on desulfurization was investigated in detail as shown in the supplementary information, Figure S2.

2.2 Materials Characterization.

The sample crystal structures were studied by powder X-ray diffraction (XRD) (Rigaku MinFlex II, Cu-Kα λ=1.5406Å). The morphologies were investigated by field-emission scanning electron microscopy (FESEM, HITACHI, SU-8010) equipped with an energy dispersive spectroscopy (EDS). The surface chemistry was analyzed by X-ray photoelectron spectroscopy (XPS, Thermo Scientific ESCALAB 250Xi).

2.3 Electrochemical Characterization.

The electrochemical performance was evaluated by using 2025-type coin cells. For the PbO/Zn aqueous battery, 2M $ZnSO_4$ was used as the electrolyte, the glass fiber membranes were used as the separators. The zinc foils with a thickness of 0.1 mm were used as negative electrodes. PbO electrodes were fabricated by blending PbO powder, Super P (H30253, 99^{+}%, Alfa Aesar), and polytetrafluoroethylene (PTFE) (Sigma Aldrich) in a weight ratio of 7:2:1. They were prepared as a sheet and then calendared on a titanium mesh (100-mesh). The obtained mesh electrodes were dried in a vacuum oven at 80 °C for 12 h. Constant current charge and discharge test and Galvanostatic Intermittent Titration Technology (GITT) were performed in LAND battery testing system (LAND CT2001A), and Cyclic voltammetry (CV) measurements were performed on CHI 760E electrochemistry workstation. Electrochemical impedance spectra of the cells were recorded on a Zahner Zennium IM6 electrochemical workstation in the frequency range of 10mHz to 100 kHz with an AC amplitude of 5 mV. The slope value in the discharge curve was calculated by fitting the 2^{nd} discharge curve between the capacity range from 5 to 105 mAh g^{-1} under the current density of 0.1A g^{-1}.

3. Results and discussion

3.1Hydrometallurgical recycling of spent LAB waste

Figure 1a shows the comparison of traditional pyrometallurgical recycle process flow and our hydrometallurgical *β*-PbO synthesizing process flow from the spent LAB waste. We cycled the lead-acid battery until the battery is completely attenuated, and then followed the industrial recycling routine to separate the lead paste for further desulfurization. In the traditional pyrometallurgical recycling, the smelting under high-temperature operation (typically

operating at 1100–1300 °C) will lead to the generation of CO_2, approximately 0.55 kg CO_2 (kg Pb)$^{-1}$ and highly toxic metal hazardous air pollutants (HAPs) [47]. While in our hydrometallurgical procedures, the obtained powder was then added to the NaOH solution for

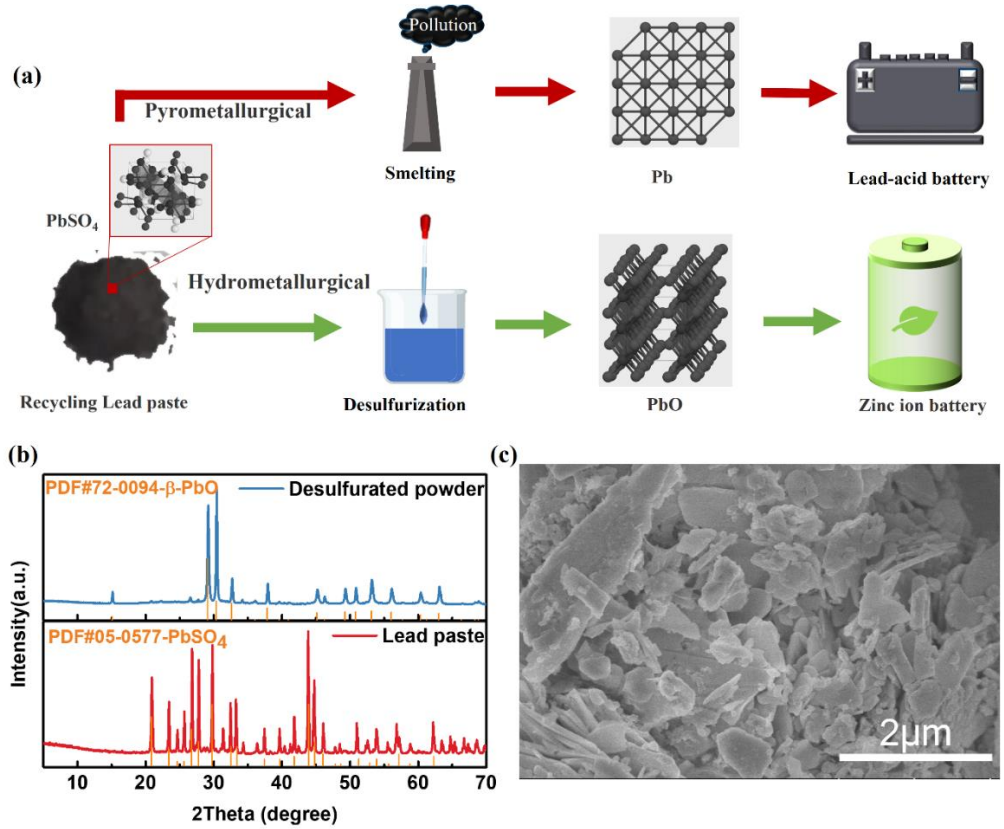

Figure 1. (a) The comparison of the traditional pyrometallurgical recycling process flow of spent LABs and the typical hydrometallurgical synthesizing process flow of *β*-PbO from the lead paste. (b) XRD pattern of the lead paste before and after hydrometallurgical treatment. (c) SEM images of the recovered lead paste.

desulfurization treatment. The desulfurized powder can be directly used in the manufacture of new ZIB batteries. According to the XRD patterns of the lead paste treated with different NaOH concentrations (Figure S2a), it is found that the crystallinity of the sample becomes worse with the increase of the concentration of NaOH desulfurizer, and some impurity's diffraction peaks (2θ=15 and 32 degrees) appear in the sample treated by 1 mol/L and 2 mol/L. Figure S2b shows the XRD patterns of the lead paste treated at different temperatures. From the figure, one can find that, with the increase of temperature from 30 °C to 60 °C, the diffraction peaks of impurity phases in the obtained PbO are eliminated. At the same time, the crystallinity of the powder treated at 60 °C is better compared with the one treated at a lower temperature. However, further

increasing the temperature to 80 ℃ results in the decrease of diffraction peak intensity and full width at half maximum (FWHM), indicating a reduced grain size in elevated temperature. By carefully selecting the desulfurization conditions, one can obtain the PbO powder with a smaller grain size which is essential for the high reversible capacity and coulombic efficiency. The XRD image of the as-disassembled lead paste and desulfurized powder using optimized conditions (80℃, 0.5mol/L NaOH) are shown in Figure 1b. From Figure 1b, one can find that the main phase of the dismantled lead paste is $PbSO_4$. After the hydrometallurgical desulfurization, the XRD of recovered lead paste shows that the main diffraction peaks match well with the orthorhombic PbO (JCPDS File Card No.72–0094). Although a small amount (< 1 wt%) of metallic lead phase can be found in the recovered lead paste, it does not affect the electrochemical performance of the assembled ZIB because the metallic lead phase can be reversibly converted into another phase as discussed in the electrochemical mechanism section. As shown in Figure S3, before desulfurization, there were Pb, O, S and C elements in the XPS survey spectrum, and the S element disappeared after desulfurization, indicating that the lead sulphate in the lead paste was successfully converted into PbO after desulfurization. The recovered lead paste has a particle size of about several micrometers as shown in the SEM images (Figure 1c and Figure S4), indicating that the simple one-step hydrometallurgical method can produce the PbO powder with a uniform size.

3.2electrochemical performance of the obtained *β*-PbO

We evaluated the electrochemical activity of PbO as ZIB material as shown in Figure 2. Figure 2a shows the cyclic voltammetry curve of the Zn/PbO cell at a scan rate of 0.1 mV s^{-1} between the voltage window of 0.02-1.6V. The sharp reduction and oxidation peaks can be found in the CV curve, located at 0.35V and 0.55V, respectively. After the first cathodic scan, the reduction peak in the CV curve moved to the higher potential region, indicating the reduced electrode polarization due to the battery activation process [48,49]. The galvanostatic discharge/charge curves are shown in Figure 2b. The discharge platform rises from the initial 0.35 V to 0.45 V after the first cycle which is consistent with the shifting of the CV reduction peak toward the higher voltage region. Moreover, the platform is very stable during the subsequent discharge process. The calculated slope value is about 0.21 mV/(mAh g^{-1}) (Figure S5). Figure 2c displays

the rate performances cycled under the current densities (0.1 to 1 A g^{-1}). From the figure, one can find that the reversible capacities with 136, 100, 92.3, and 78.4 mAh g^{-1} are obtained under the current densities of 0.1, 0.3, 0.5, and 1.0 A g^{-1}, respectively. The charge/discharge profiles with different current densities are plotted in Figure 2d. It is found that all the charge-discharge curves consist of a stable charge-discharge platform. Besides, the long-term stability of PbO also has been evaluated at 1A g^{-1} (Figure 2e), and the battery can deliver a stable capacity during the first 200 cycles. The charge and discharge curves of different cycles at 1A g^{-1} current density are shown in Figure S6. The flat platforms can be observed at each cycle.

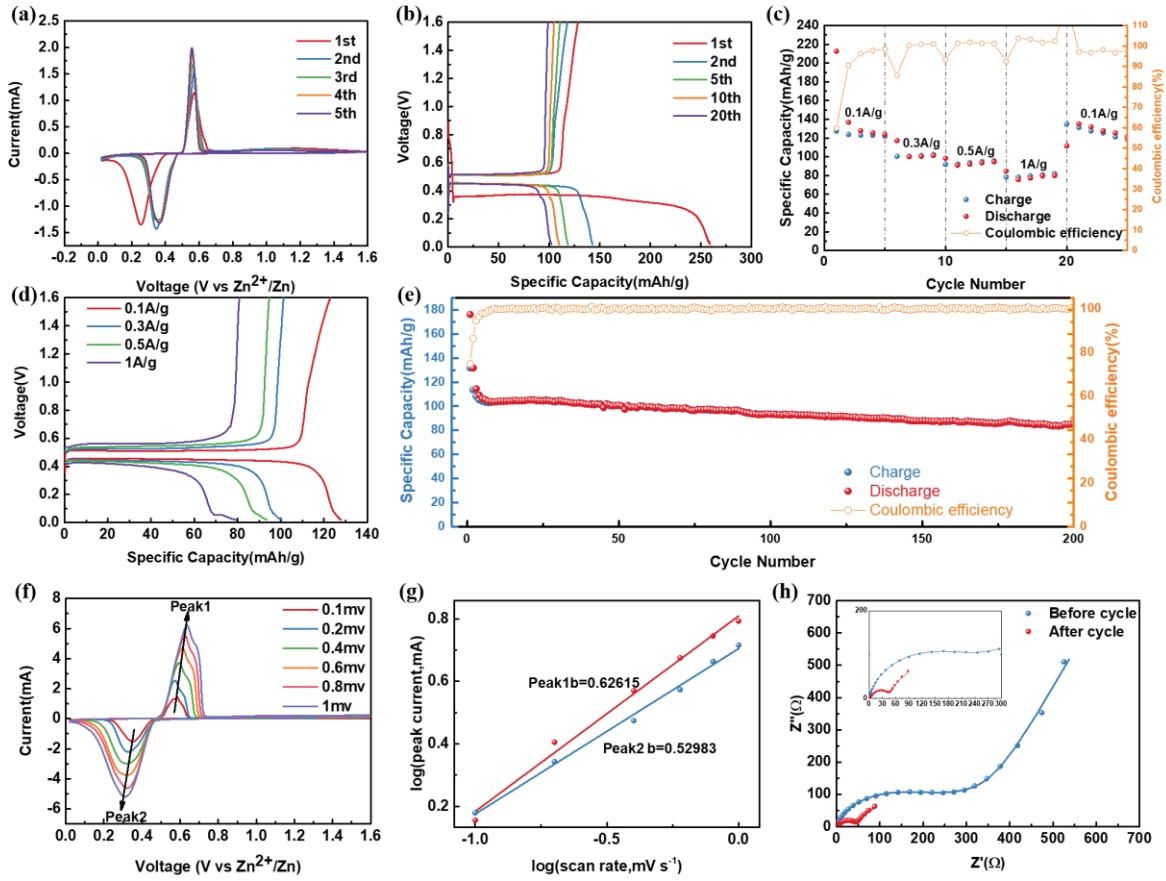

Figure 2. Electrochemical performances of PbO electrode. (a) CV curves at scanning rate of 0.1 mV s^{-1}; (b) The discharge/charge curves at 0.1 A g^{-1}. (c) Rate capabilities and (d) charge/discharge curves at different current densities. (e) Cyclic performances at 1A g^{-1} between 0.02 and1.6 V. (f) CV curves with scan rates of 0.1 to 1.0 mV s^{-1} between 0.02 and 1.6V; (g) The corresponding plots of log(i) versus log(v) at the redox peaks shown in (f); (h) AC impedance spectra of the PbO electrode before and after cycling.

To understand the Zn^{2+} storage kinetics inside the PbO cathode, the cyclic voltammetry

measurements (Figure 2f) were conducted at different scan rates from 0.1 to 1 mV s^{-1}. Two peaks are observed in every curve. With the increase of scanning rates, the reduction peak moves to the lower potential direction, and the oxidation peak moves to the higher voltage region. The relation between the peak currents (i) and scan rates (v) can be described as following [50,51]

$$i = av^b \tag{1}$$

which can be equally written as

$$\log(i) = b\log(v) + \log(a) \tag{2}$$

Where b is defined as the slope of log(i) versus log(v) curve. In general, the value of b with 0.5-1 is related to the type of electrochemical process. When the b value reaches 0.5, the electrochemical kinetic process is dominated by ion diffusion. When the value of b is 1, the surface capacitance effect is the dominant contributor to the CV current. From Figure 2g, it can be obtained that the b values for peak 1 and peak 2 are 0.626 and 0.529 respectively, which means that the charge transfer is dominated by the ion diffusion process. In the Nyquist diagrams (Figure 2h), in the high frequency region, the impedance plots for batteries before and after the cycle are both composed of semicircles corresponding to the charge transfer impedance (R_{ct}). The fitting model and R_{ct} values are shown in Figure S7 and Table S1, The dramatic decrease of the R_{ct} value, from about 197 ohms to 48.9 ohms, is closely related to the battery's initial activation process. This agrees well with the increased discharge platform voltage in Figure 2b.

3.3 Charge transfer and storage mechanism

The ultra-flat platform in the PbO electrode differs significantly from that of traditional zinc ion batteries, which implies its charge storage mechanism should be different from the traditional Zn^{2+}/proton intercalation mechanism. We further performed the *ex-situ* XRD measurements to understand the reaction mechanism of PbO electrodes. The *ex-situ* XRD patterns recorded the electrode crystal structure at different charge and discharge states during the first cycle as shown in Figure 3a. Initially, β-phase PbO is observed before the cell stabilization, while only $PbSO_4$ and $(ZnSO_4)[Zn(OH)_2]_3 \cdot 5H_2O$ (ZHS) are observed as long as

the cell voltage entered the discharge platform at around 0.4 V. Further reduce the cell voltage, the diffraction peaks intensity of $PbSO_4$ are gradually reduced, and the Pb peaks intensity increase and become the dominating phase. At the end of the first discharge, the $PbSO_4$ phase

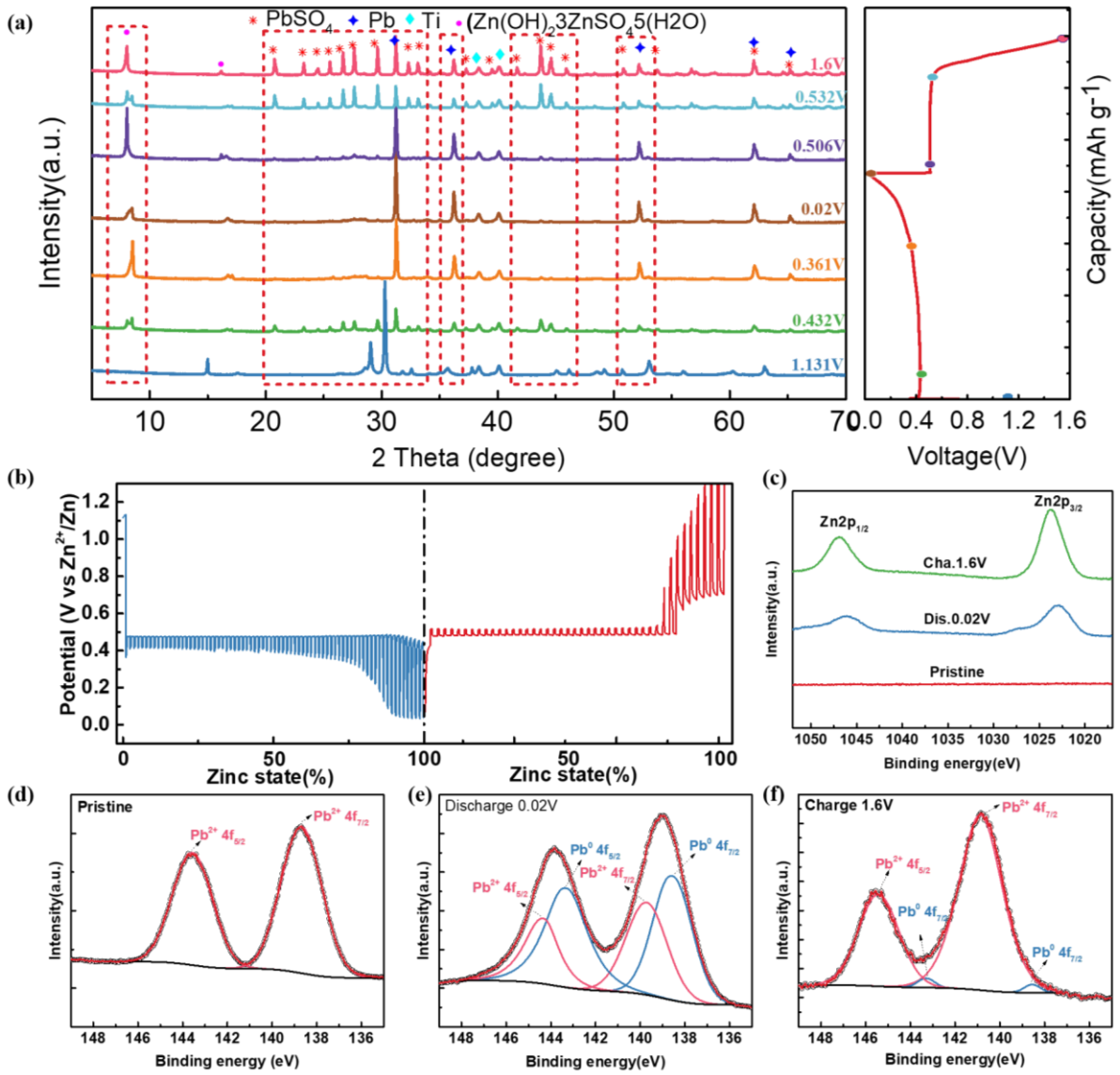

Figure 3. (a) *Ex-situ* XRD patterns of PbO electrode at different charge/discharge stages. (b)The first GITT cycle for Zn–PbO system. (c) Zn2p XPS spectrum of electrode surface at different cycle states (cycle current density ~ 0.1A g^{-1}). Pb4f XPS spectra for the (d) pristine, (e) fully discharged, and (f) fully charged electrodes, respectively.

is fully converted as the Pb phase. By contrast, during the charging process, the $PbSO_4$ peaks re-appear accompanied by the decrease of Pb peak intensity. It is also worth noting that the

reversible increase/decrease of ZHS phase diffraction peak intensity was also found within the first cycle. The ZHS phase is sensitive to the PH value of the electrolyte, and the OH^- in ZHS mainly comes from the self-ionization of water molecules in the electrolyte. The initial cell stabilization process of the PbO electrode consumed H^+ and SO_4^{2-} to generate $PbSO_4$, Therefore, the consumption of H^+ could, in turn, generate an OH^- rich region on top of the electrode surface, resulting in the formation of ZHS. The above results indicate that the charge storage in the PbO electrode is based on the reversible transfer between the $PbSO_4$ and Pb. Importantly, this reversible transfer can only occur with the assistance of the formation and dissolution of ZHS on the electrode surface (see detailed discussion in section 3.4). Hence, the electrochemical reactions of the aqueous Zn/PbO batteries can be summarized below,

Battery stabilization:

$$PbO + 2H^+ + SO_4^{2-} \rightarrow PbSO_4 + H_2O \quad (3)$$

$$3Zn^{2+} + 6OH^- + ZnSO_4 + 5H_2O \rightarrow (ZnSO_4)[Zn(OH)_2]_3 \cdot 5H_2O\downarrow \quad (4)$$

Positive electrode:

$$PbSO_4 + H^+ + 2e^- \underset{Discharge}{\overset{Charge}{\longleftrightarrow}} Pb + HSO_4^- \quad (5)$$

$$4Zn^{2+} + 6OH^- + SO_4^{2-} + 5H_2O \underset{Discharge}{\overset{Charge}{\longleftrightarrow}} (ZnSO_4)[Zn(OH)_2]_3 \cdot 5H_2O\downarrow \quad (6)$$

Negative electrode:

$$Zn \underset{Discharge}{\overset{Charge}{\longleftrightarrow}} Zn^{2+} + 2e^- \quad (7)$$

Galvanostatic intermittent titration technique (GITT) was used to study the dynamic process and equilibrium potential of PbO during discharging and charging. Figure 3b shows the GITT for PbO-Zn battery, with current pulses of 0.05 A g^{-1} for 10 min followed by a relaxation step for 30 min. From the figure, one can notice that the voltage enters a quasi-balanced state after each pulse. Astonishingly, the quasi-equilibrium potentials during discharge and charge are very stable, and they lie on two horizontal lines between 0.47-0.51V. The flat and stable equilibrium platforms indicate the existence of a two-phase coexistence region [52,53]. The small potential gap (0.04V) indicates the high reversibility and small energy barrier of $PbSO_4$

↔ Pb transformation. Based on the ex-XRD and GITT results, one can conclude that the ultra-flat plateau should derive from the two-phase transformation between Pb and $PbSO_4$.

Figure 3c is the XPS spectra of Zn2p in the first discharge and charge states. Two Zn2p peaks can be observed in the fully discharge/charge electrode, indicating the formation of ZHS on the electrode surface. The small peak at binding energy 127.3eV should derive from the chemical environment formed between Zn^{2+} and anions in the active electrode material [54] due to the higher electronegativity. Figure S8 shows the XPS survey spectra of the PbO electrode at pristine, discharge and charge states, Figures 3(d), (e) and (f) show Pb4f spectra for the pristine, fully discharged and fully charged electrodes, respectively. For the pristine electrode, the valence state of Pb is +2, and the peaks in the curve correspond to the binding energy position of Pb-O($4f_{5/2}$) and Pb-O($4f_{7/2}$) [55]. In the full discharge state, two peaks at 138.5eV ($Pb4f_{7/2}$) and 143.3eV ($Pb4f_{5/2}$) can be assigned to metallic Pb, and the two peaks at 139.7eV ($Pb4f_{7/2}$) and 144.3eV ($Pb4f_{5/2}$) correspond to $PbSO_4$ [55,56]. The reduced ratio of Pb^{+2} vs metallic Pb in the lead element spectra confirms that Pb^{+2} is reduced into metallic Pb during the discharge. In the fully charged state, the Pb4f spectrum shows mainly the Pb^{+2} signal, confirming the high reversibility of the electrochemical transformation between the $PbSO_4$ and Pb phases. This is consistent with *ex-situ* XRD and GITT results that PbO is reduced to Pb during the first discharge, and the subsequent conversion reaction between Pb and $PbSO_4$ contributes the most Battery capacity.

3.4 The effects of ZHS on battery performance.

To further understand the role of ZHS in the charging and discharging process of the Zn/PbO battery, we performed a detailed SEM characterization of the surface morphology of the PbO electrode at different potentials during the first cycle (Figures 4a-g). At a discharge voltage of ~0.43 V, many hexagonal nanosheets are observed on the electrode surface, and the sizes of these nanosheets increase when the discharge reaches ~0.36 V. However, the nanosheets gradually disappear at the full discharge state. During the charging process, at the voltage platform at around 0.4 V, the numbers of nanosheets increase again, but gradually

disappear upon the charging progresses. The SEM-EDS mapping (Figure 4h) of a typical nanosheet shows that the Zn, O and S elements uniformly distribute inside the nanosheet, indicating that these observed nanosheets are ZHS [57]. This is consistent with the XRD patterns in Figure 3. It further proves the proposed reaction mechanism based on equations (6).

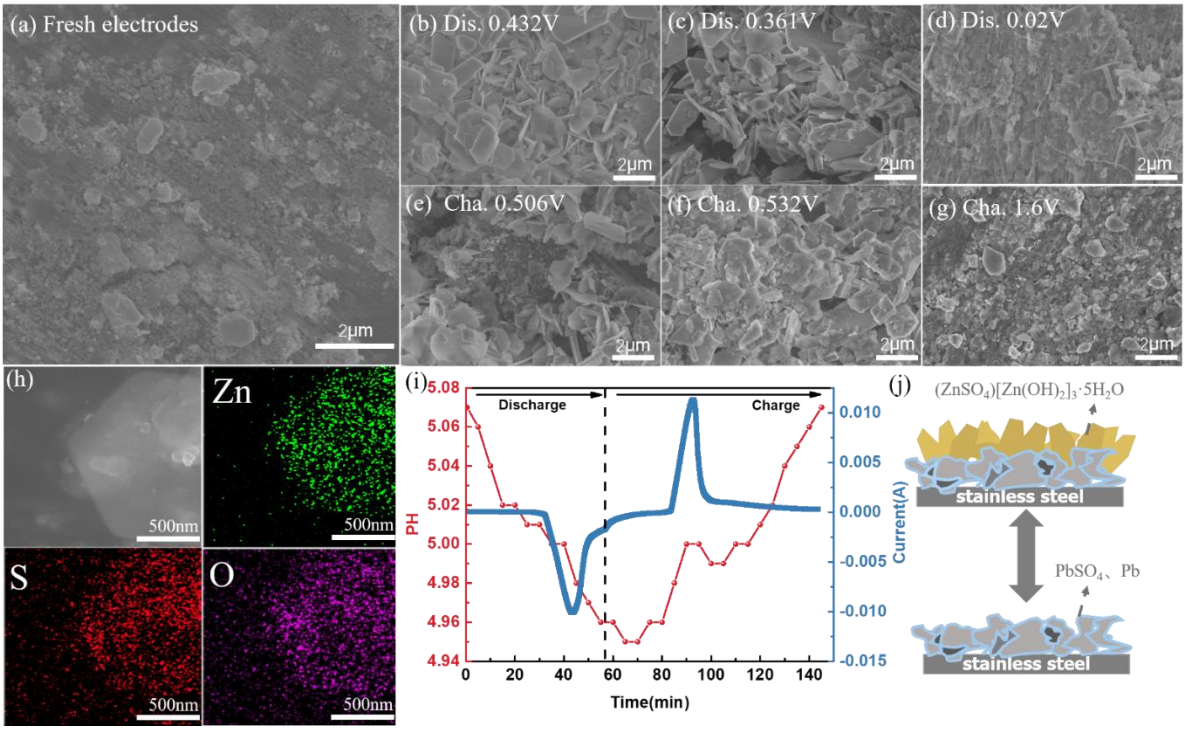

Figure 4. Characterization results of PbO cathode during the first charge and discharge cycle. (a-g) SEM images of the cathode surface at different charge and discharge states. (h) EDS mapping of the generated ZHS nanosheets on the electrode surface.in-situ pH changes of Zn//PbO. (i) in-situ pH changes of Zn//PbO. (j) Sketch mode of the reversible conversion with the assistance of ZHS passivation layer.

The change of H^+ concentration in the electrolyte is the direct evidence of the proton reaction, therefore *in situ* pH measurements were used to determine pH evolution during discharge and charging. As shown in Figure 4i, the pH value changes continuously, from 5.07 to 4.95 during the cathodic scan (0-70 mins) and from 4.95 to 5.07 during the anodic scan (70-140 mins). The dramatic change in the pH of the electrolyte indicates that protons participate in the electrode reaction, which is consistent with the previous report on MnO_2/Zn system [58,59]. According to equation (5), the conversion between the Pb and Pb^{2+} requires a reversible accumulation and

dissipation of protons on the electrode surface as shown in Figure 4j. It is the reversible formation and dissolution of the ZHS solid-state interphase (SEI) layer that enables the effective tuning of pH values on the electrode-electrolyte interface, which results in the highly stable and charge transformation between the Pb and Pb^{2+}. As a comparison, by changing the electrolyte from $ZnSO_4$ to $Zn(CF_3SO_3)_2$ to inhibit the formation of ZHS, we found that the absence of ZHS on the PbO electrode surface can barely deliver any capacity (Figure S9). It is also worth noting that using $PbSO_4$ directly as the active material will also avoid the formation of ZHS during battery stabilization. However, the $PbSO_4$ without the ZHS suffered from serious capacity degradation during the initial cycles (Figure S10). Therefore, based on the *ex-situ* XRD and SEM observation results, one can conclude the reversible ZHS formation on the electrode surface can effectively regulate the proton concentration on the electrode surface, which reduced the energy barriers and enhance the reversibility of the electrochemical conversion between Pb^{2+} and metallic Pb.

4. Conclusion

In conclusion, we report a simple hydrometallurgical recycling method for the LAB lead paste waste to obtain the β-PbO byproduct as a novel ZIB active material. PbO was first tested as the active material of aqueous ZIB. The ultra-flat characteristic of charge/discharge platforms of PbO/Zn battery was found for the first time, which can be attributed to the reversible conversion between Pb and $PbSO_4$ phases. Moreover, the reaction mechanism was confirmed by *ex-situ* XRD, XPS, SEM and *in-situ* PH measurements. We found that the PbO exhibits a unique energy storage mechanism, the conversion reaction of Pb and $PbSO_4$ contributes most of the battery capacity with the assistance of ZHS as SEI layer to regulate the electrode surface proton concentrations. This work broadens the choice of electrode active materials for aqueous zinc ion batteries and inspires searching for new materials with ultra-flatten voltage platforms.

Authorship contribution statement

Chun Lin: Investigation, Conceptualization, Methodology, Writing – original draft. **Yue Chen**: Investigation, Data curation, Formal analysis, Supervision, Writing – review & editing.

Weijian Zhang: Data curation, Visualization, Investigation. **Jiaxin Li**: Validation, Investigation, Supervision, Project administration, Funding acquisition. **Yingbin Lin**: Investigation, Resources, Formal analysis. **Oleg V. Kolosov**: Methodology, Resources, Writing – review & editing, Funding acquisition. **Zhigao Huang**: Conceptualization, Writing – review & editing, Project administration, Funding acquisition.

Declaration of Competing Interest

The authors declare that they have no known competing financial interests or personal relationships that could have appeared to influence the work reported in this paper.

Acknowledgements

The authors wish to acknowledge the financial support by the Natural Science Foundations of China (No. 61574037, 11344008, 11204038, 22179020), Foreign science and technology cooperation project of Fuzhou Science and Technology Bureau (No. 2021-Y-086), Industry-university Cooperation Project of Fujian Province (No. 2020H06027), the Faraday Institution (grant number FIRG018), and EPSRC project EP/V00767X/1.

References

[1] J.M. Tarascon, M. Armand, Issues and challenges facing rechargeable lithium batteries. Nature 414(2001) 359-367. https://doi.org/10.1142/9789814317665_0024

[2] H. Li, Z. Wang, L. Chen, X. Huang, Research on Advanced Materials for Li-ion Batteries, Adv. Mater., 21 (2009) 4593-4607. https://doi.org/10.1002/adma.200901710

[3] J.B. Goodenough, Y. Kim, Challenges for Rechargeable Li Batteries†, Chem. Mater., 22 (2010) 587-603. https://doi.org/10.1021/cm901452z

[4] J.B. Goodenough, K.S. Park, The Li-ion rechargeable battery: a perspective, J. Am. Chem. Soc, 135 (2013) 1167-1176. https://doi.org/10.1021/ja3091438

[5] W. He, F.J. Ye, J. Lin, Q. Wang, Q.S. Xie, F. Pei, C.Y. Zhang, P.F. Liu, X.W. Li, L.S. Wang, B.H. Qu, D.L. Peng, Boosting the Electrochemical Performance of Li- and Mn-Rich Cathodes by a Three-in-One Strategy, Nano-Micro Letters, 13 (2021) 205. https://doi.org/10.1007/s40820-021-00725-0

[6] V. Etacheri, R. Marom, R. Elazari, G. Salitra, D. Aurbach, Challenges in the development of advanced Li-ion batteries: a review, Energy Environ. Sci., 4 (2011) 3243-3250. https://doi.org/10.1039/C1EE01598B

[7] J.L. Ma, F.L. Meng, Y. Yu, D.P. Liu, J.M. Yan, Y. Zhang, X.B. Zhang, Q. Jiang, Prevention of dendrite growth and volume expansion to give high-performance aprotic bimetallic Li-Na alloy-O_2 batteries, Nat. Chem., 11 (2019) 64-70. https://doi.org/10.1038/s41557-018-0166-9

[8] B. Tang, L. Shan, S. Liang, J. Zhou, Issues and opportunities facing aqueous zinc-ion batteries, Energy Environ. Sci., 12 (2019) 3288-3304. https://doi.org/10.1039/C9EE02526J

[9] J. Ming, J. Guo, C. Xia, W. Wang, H.N. Alshareef, Zinc-ion batteries: Materials, mechanisms, and applications, Materials Science and Engineering: R: Reports, 135 (20 19) 58-84. https://doi.org/10.1016/j.mser.2018.10.002

[10] D. Kundu, B.D. Adams, V. Duffort, S.H. Vajargah, L.F. Nazar, A high-capacity a nd long-life aqueous rechargeable zinc battery using a metal oxide intercalation cathod e, Nat. Energy, 1 (2016) 16119. https://doi.org/10.1038/nenergy.2016.119

[11] Q. Zhang, Y.P. Zeng, C.S. Ling, L Wang, Z.Y. Wang, T.E. Fan, H Wang, J.R. X iao, B.H. Qu, Boosting Fast Sodium Ion Storage by Synergistic Effect of Heterointerf ace Engineering and Nitrogen Doping Porous Carbon Nanofibers, Small, 18 (2022) 21 07514. https://doi.org/10.1002/smll.202107514

[12] B. Liu, D.N. Lei, J. Wang, Q.F. Zhang, W. He, H.F. Zheng, B.S. Sa, Q.S. Xi, D.L. Peng, B.H. Qu, 3D uniform nitrogen-doped carbon skeleton for ultra-stable sodium metal anode. Nano Research, 13 (2020) 2136-2142. https://doi.org/10.1007/s12274-020-2820-y

[13] P. Yu, Y. Zeng, H. Zhang, M. Yu, Y. Tong, X. Lu, Flexible Zn-Ion Batteries: Recent Progresses and Challenges, Small, 15 (2019) e1804760. https://doi.org/10.1002/smll.201804760

[14] X. Zeng, J. Hao, Z. Wang, J. Mao, Z. Guo, Recent progress and perspectives on aqueous Zn-based rechargeable batteries with mild aqueous electrolytes, Energy Stora ge Mater., 20 (2019) 410-437. https://doi.org/10.1016/j.ensm.2019.04.022

[15] G. Fang, J. Zhou, A. Pan, S. Liang, Recent Advances in Aqueous Zinc-Ion Batteries, ACS Energy Lett., 3 (2018) 2480-2501. https://doi.org/10.1021/acsenergylett.8b01426

[16] C. Xu, B. Li, H. Du, F. Kang, Energetic Zinc Ion Chemistry: The Rechargeable Zinc Ion Battery, Angew. Chem. Int. Ed., 51 (2012) 933-935. https://doi.org/10.1002/ange.201106307

[17] W. Xu, Y. Wang, Recent Progress on Zinc-Ion Rechargeable Batteries, Nano-Micro Lett.,

11 (2019). https://doi.org/10.1007/s40820-019-0322-9

[18] N. Zhang, F. Cheng, J. Liu, L. Wang, X. Long, X. Liu, F. Li, J. Chen, Recharg eable aqueous zinc-manganese dioxide batteries with high energy and power densities, Nat. Commun., 8 (2017) 405. https://doi.org/10.1038/s41467-017-00467-x

[19] H. Pan, Y. Shao, P. Yan, Y. Cheng, K.S. Han, Z. Nie, C. Wang, J. Yang, X. Li, P. Bhattacharya, K.T. Mueller, J. Liu, Reversible aqueous zinc/manganese oxide energy storage from conversion reactions, Nat. Energy, 1 (2016) 16039. https://doi.org/10.1038/nenergy.2016.39

[20] W. Sun, F. Wang, S. Hou, C. Yang, X. Fan, Z. Ma, T. Gao, F. Han, R. Hu, M. Zhu, C. Wang, Zn/MnO_2 Battery Chemistry With H^+ and Zn^{2+} Coinsertion, J. Am. C hem. Soc., 139 (2017) 9775-9778. https://doi.org/10.1021/jacs.7b04471

[21] C. Wei, C. Xu, B. Li, H. Du, F. Kang, Preparation and characterization of mang anese dioxides with nano-sized tunnel structures for zinc ion storage, J. Phys. Chem. Solids, 73 (2012) 1487-1491. https://doi.org/10.1016/j.jpcs.2011.11.038

[22] B. Wu, G. Zhang, M. Yan, T. Xiong, P. He, L. He, X. Xu, L. Mai, Graphene Scroll-Coated alpha-MnO_2 Nanowires as High-Performance Cathode Materials for Aqueous Zn-Ion Battery, Small, 14 (2018) e1703850. https://doi.org/10.1002/smll.201703850

[23] N. Liu, X. Wu, Y. Yin, A. Chen, C. Zhao, Z. Guo, L. Fan, N. Zhang, Constructing the Efficient Ion Diffusion Pathway by Introducing Oxygen Defects in Mn_2O_3 for High-Performance Aqueous Zinc-Ion Batteries, ACS Appl. Mater. Interfaces, 12 (2020) 28199-28205. https://doi.org/10.1021/acsami.0c05968

[24] J. Hao, J. Mou, J. Zhang, L. Dong, W. Liu, C. Xu, F. Kang, Electrochemically induced spinel-layered phase transition of Mn_3O_4 in high performance neutral aqueous rechargeable zinc battery, Electrochim. Acta, 259 (2018) 170-178. https://doi.org/10.1016/j.electacta.2017.10.166

[25] H. Chen, W. Zhou, D. Zhu, Z. Liu, Z. Feng, J. Li, Y. Chen, Porous cube-like Mn_3O_4@C as an advanced cathode for low-cost neutral zinc-ion battery, J. Alloys Co mpd., 813 (2020) 151812. https://doi.org/10.1016/j.jallcom.2019.151812

[26] L. Chen, Z. Yang, H. Qin, X. Zeng, J. Meng, Advanced electrochemical performance of

$ZnMn_2O_4$/N-doped graphene hybrid as cathode material for zinc ion battery, J. Power Sources, 425 (2019) 162-169. https://doi.org/10.1016/j.jpowsour.2019.04.010

[27] J. Ding, Z. Du, L. Gu, B. Li, L. Wang, S. Wang, Y. Gong, S. Yang, Ultrafast Zn^{2+} Intercalation and Deintercalation in Vanadium Dioxide, Adv. Mater., 30 (2018) e1800762. https://doi.org/10.1002/adma.201800762

[28] J. Zhou, L. Shan, Z. Wu, X. Guo, G. Fang, S. Liang, Investigation of V_2O_5 as a low-cost rechargeable aqueous zinc ion battery cathode, Chem. Commun. (Camb.), 54 (2018) 4457-4460. https://doi.org/10.1039/C8CC02250J

[29] Y. Li, Z. Huang, P.K. Kalambate, Y. Zhong, Z. Huang, M. Xie, Y. Shen, Y. Huang, V_2O_5 nanopaper as a cathode material with high capacity and long cycle life for rechargeable aqueous zinc-ion battery, Nano Energy, 60 (2019) 752-759. https://doi.org/10.1016/j.nanoen.2019.04.009

[30] P. He, G. Zhang, X. Liao, M. Yan, X. Xu, Q. An, J. Liu, L. Mai, Sodium Ion Stabilized Vanadium Oxide Nanowire Cathode for High-Performance Zinc-Ion Batteries, Adv. Energy Mater., 8 (2018) 1702463. https://doi.org/10.1002/aenm.201702463

[31] C. Xia, J. Guo, P. Li, X. Zhang, H.N. Alshareef, Highly Stable Aqueous Zinc-Ion Storage Using a Layered Calcium Vanadium Oxide Bronze Cathode, Angew. Chem. Int. Ed. Engl., 57 (2018) 3943-3948. https://doi.org/10.1002/anie.201713291

[32] M.H. Alfaruqi, V. Mathew, J. Song, S. Kim, S. Islam, D.T. Pham, J. Jo, S. Kim, J.P. Baboo, Z. Xiu, K.-S. Lee, Y.-K. Sun, J. Kim, Electrochemical Zinc Intercalation in Lithium Vanadium Oxide: A High-Capacity Zinc-Ion Battery Cathode, Chem. Mater., 29 (2017) 1684-1694. https://doi.org/10.1021/acs.chemmater.6b05092

[33] B. Sambandam, V. Soundharrajan, S. Kim, M.H. Alfaruqi, J. Jo, S. Kim, V. Mathew, Y.-k. Sun, J. Kim, Aqueous rechargeable Zn-ion batteries: an imperishable and high-energy $Zn_2V_2O_7$ nanowire cathode through intercalation regulation, J. Mater. Chem. A, 6 (2018) 3850-3856. https://doi.org/10.1039/C7TA11237H

[34] G. Li, Z. Yang, Y. Jiang, W. Zhang, Y. Huang, Hybrid aqueous battery based on $Na_3V_2(PO_4)_3$/C cathode and zinc anode for potential large-scale energy storage, J. Power Sources, 308 (2016) 52-57. https://doi.org/10.1016/j.jpowsour.2016.01.058

[35] M.S. Chae, J.W. Heo, S.C. Lim, S.T. Hong, Electrochemical Zinc-Ion Intercalation Properties and Crystal Structures of $ZnMo_6S_8$ and $Zn_2Mo_6S_8$ Chevrel Phases in Aqueous Electrolytes, Inorg. Chem., 55 (2016) 3294-3301. https://doi.org/10.1021/acs.inorgchem.5b02362

[36] Y. Cheng, L. Luo, L. Zhong, J. Chen, B. Li, W. Wang, S.X. Mao, C. Wang, V. L. Sprenkle, G. Li, J. Liu, Highly Reversible Zinc-Ion Intercalation into Chevrel Phase Mo_6S_8 Nanocubes and Applications for Advanced Zinc-Ion Batteries, ACS Appl. Mater. Interfaces, 8 (2016) 13673-13677. https://doi.org/10.1021/acsami.6b03197

[37] P. Hu, T. Zhu, X. Wang, X. Wei, M. Yan, J. Li, W. Luo, W. Yang, W. Zhang, L. Zhou, Z. Zhou, L. Mai, Highly Durable $Na_2V_6O_{16}.1.63H_2O$ Nanowire Cathode for Aqueous Zinc-Ion Battery, Nano Lett., 18 (2018) 1758-1763. https://doi.org/10.1021/acs.nanolett.7b04889

[38] V. Soundharrajan, B. Sambandam, S. Kim, M.H. Alfaruqi, D.Y. Putro, J. Jo, S. Kim, V. Mathew, Y.K. Sun, J. Kim, $Na_2V_6O_{16}.3H_2O$ Barnesite Nanorod: An Open Door to Display a Stable and High Energy for Aqueous Rechargeable Zn-Ion Batteries as Cathodes, Nano Lett., 18 (2018) 2402-2410. https://doi.org/10.1021/acs.nanolett.7b05403

[39] H. Chen, T.N. Cong, W. Yang, C. Tan, Y. Li, Y. Ding, Progress in electrical energy storage system: A critical review, Prog. Nat. Sci., 19 (2009) 291-312.

[40] Y.-H. Zhu, Q. Zhang, X. Yang, E.-Y. Zhao, T. Sun, X.-B. Zhang, S. Wang, X.-Q. Yu, J.-M. Yan, Q. Jiang, Reconstructed Orthorhombic V_2O_5 Polyhedra for Fast Ion Diffusion in K-Ion Batteries, Chem., 5 (2019) 168-179. https://doi.org/10.1016/j.chempr.2018.10.004

[41] S. Wang, X.B. Zhang, N-Doped C@$Zn_3B_2O_6$ as a Low Cost and Environmentally Friendly Anode Material for Na-Ion Batteries: High Performance and New Reaction Mechanism, Adv. Mater., 31 (2019) e1805432. https://doi.org/10.1002/adma.201805432

[42] S. Mandal, S. Thangarasu, P.T. Thong, S.-C. Kim, J.-Y. Shim, H.-Y. Jung, Positive electrode active material development opportunities through carbon addition in the lead-acid batteries: A recent progress, J. Power Sources, 485 (2021) 229336. https://doi.org/10.1016/j.jpowsour.2020.229336

[43] M. Li, J. Yang, S. Liang, H. Hou, J. Hu, B. Liu, R.V. Kumar, Review on clean

recovery of discarded/spent lead-acid battery and trends of recycled products, J. Power Sources, 436 (2019) 226853. https://doi.org/10.1016/j.jpowsour.2019.226853

[44] W. Zhang, J. Yang, X. Wu, Y. Hu, W. Yu, J. Wang, J. Dong, M. Li, S. Liang, J. Hu, R.V. Kumar, A critical review on secondary lead recycling technology and its prospect, Renewable Sustainable Energy Rev., 61 (2016) 108-122. https://doi.org/10.1016/j.rser.2016.03.046

[45] Y. Hu, J. Yang, J. Hu, J. Wang, S. Liang, H. Hou, X. Wu, B. Liu, W. Yu, X. He, R.V. Kumar, Synthesis of Nanostructured PbO@C Composite Derived from Spent Lead-Acid Battery for Next-Generation Lead-Carbon Battery, Adv. Funct. Mater., 28 (2018) 1705294. https://doi.org/10.1002/adfm.201705294

[46] X. He, X. Peng, Y. Zhu, C. Lai, C. Ducati, R.V. Kumar, Producing hierarchical porous carbon monoliths from hydrometallurgical recycling of spent lead acid battery for application in lithium ion batteries, Green Chem., 17 (2015) 4637-4646. https://doi.org/10.1039/C5GC01203A

[47] A.J. Davidson, S.P. Binks, J. Gediga, Lead industry life cycle studies: environmental impact and life cycle assessment of lead battery and architectural sheet production, The International Journal of Life Cycle Assessment, 21 (2016) 1624-1636. https://doi.org/10.1007/s11367-015-1021-5

[48] J. Meng, Z. Yang, L. Chen, H. Qin, F. Cui, Y. Jiang, X. Zeng, Energy storage performance of CuO as a cathode material for aqueous zinc ion battery, Mater. Today Energy, 15 (2020) 100370. https://doi.org/10.1016/j.mtener.2019.100370

[49] Y. Fu, Q. Wei, G. Zhang, X. Wang, J. Zhang, Y. Hu, D. Wang, L. Zuin, T. Zhou, Y. Wu, S. Sun, High-Performance Reversible Aqueous Zn-Ion Battery Based on Porous MnO_x Nanorods Coated by MOF-Derived N-Doped Carbon, Adv. Energy Mater., 8 (2018) 1801445. https://doi.org/10.1002/aenm.201801445

[50] K. Zhang, M. Park, L. Zhou, G.-H. Lee, W. Li, Y.-M. Kang, J. Chen, Urchin-Li ke $CoSe_2$ as a High-Performance Anode Material for Sodium-Ion Batteries, Adv. Func t. Mater., 26 (2016) 6728-6735. https://doi.org/10.1002/adfm.201602608

[51] D. Chao, C. Zhu, P. Yang, X. Xia, J. Liu, J. Wang, X. Fan, S.V. Savilov, J. Lin, H.J. Fan, Z.X. Shen, Array of nanosheets render ultrafast and high-capacity Na-ion storage by tunable

pseudocapacitance, Nat. Commun., 7 (2016) 12122. https://doi.org/10.1038/ncomms12122

[52] D. Wang, Y. Zhao, G. Liang, F. Mo, H. Li, Z. Huang, X. Li, T. Tang, B. Dong, C. Zhi, A zinc battery with ultra-flat discharge plateau through phase transition mech anism, Nano Energy, 71 (2020) 104583. https://doi.org/10.1016/j.nanoen.2020.104583

[53] Y.J. Zhu, C.S. Wang, Galvanostatic intermittent titration technique for phase-transformation electrodes. J. Phys. Chem. Lett., 114(2010) 2830-2841. https://doi.org/10.1021/jp9113333

[54] T. Xiong, Y. M. Wang, B. S. Yin, W. Shi, W. S. V. Lee, J. M. Xue, Bi_2S_3 for Aqueous Zn Ion Battery with Enhanced Cycle Stability, Nano-Micro Letters 12, (2020). https://doi.org/10.1007/s40820-019-0352-3

[55] X. Huang, J. Song, H. Wu, C. Xie, M. Hua, Y. Hu, B. Han, Ordered-Mesoporous-Carbon-Confined Pb/PbO Composites: Superior Electrocatalysts for CO_2 Reduction, ChemSusChem, 13 (2020) 6346-6352. https://doi.org/10.1002/cssc.202000329

[56] D.S. Zingg, D.M. Hercules, Electron spectroscopy for chemical analysis studies of lead sulfide oxidation. J. Phys. Chem. C. 82(1978) 1992-1995. https://doi.org/10.1021/j100507a008

[57] T. Zhang, Y. Tang, G. Fang, C. Zhang, H. Zhang, X. Guo, X. Cao, J. Zhou, A. Pan, S. Liang, Electrochemical Activation of Manganese-Based Cathode in Aqueous Zinc-Ion Electrolyte, Adv. Funct. Mater., 30 (2020) 2002711. https://doi.org/10.1002/adfm.202002711

[58] H. Chen, S. Cai, Y. Wu, W. Wang, M. Xu, S.J. Bao, Successive electrochemical conversion reaction to understand the performance of aqueous Zn/MnO_2 batteries with Mn^{2+} additive, Mater. Today Energy, 20 (2021) 100646. https://doi.org/10.1016/j.mtener.2021.100646

[59] B. Lee, J. Choi, M. Lee, S. Han, M. Jeong, T. Yim, S.H. Oh, Unraveling the cr itical role of Zn-phyllomanganates in zinc ion batteries, J. Mater. Chem. A, 9 (2021) 13950-13957. https://doi.org/10.1039/D1TA03536C